HHS Public Access

Author manuscript

Clin Neurophysiol. Author manuscript; available in PMC 2019 January 01.

Published in final edited form as:

Clin Neurophysiol. 2018 January ; 129(1): 188–197. doi:10.1016/j.clinph.2017.10.019.

Four-dimensional map of the human early visual system

Yasuo Nakai[1,4], **Akari Nagashima**[1], **Akane Hayakawa**[1], **Takuya Osuki**[1], **Jeong-won Jeong**[1,2], **Ayaka Sugiura**[1], **Erik C Brown**[3], and **Eishi Asano**[1,2,*]

[1]Department of Pediatrics, Wayne State University, Children's Hospital of Michigan, Detroit Medical Center, Detroit, MI, 48201, USA

[2]Department of Neurology, Wayne State University, Children's Hospital of Michigan, Detroit Medical Center, Detroit, MI, 48201, USA

[3]Department of Neurological Surgery, Oregon Health and Science University, Portland, OR, 97239, USA

[4]Department of Neurological Surgery, Wakayama Medical University, Wakayama-shi, Wakayama, 6418510, JAPAN

Abstract

OBJECTIVE—We generated a large-scale, four-dimensional map of neuronal modulations elicited by full-field flash stimulation.

METHODS—We analyzed electrocorticography (ECoG) recordings from 63 patients with focal epilepsy, and delineated the spatial-temporal dynamics of visually-elicited high-gamma$_{70–110\ Hz}$ amplitudes on a standard brain template. We then clarified the neuronal events underlying visual evoked potential (VEP) components, by correlating with high-gamma amplitude measures.

RESULTS—The medial-occipital cortex initially revealed rapid neural activation followed by prolonged suppression, reflected by augmentation of high-gamma activity lasting up to 100 ms followed by attenuation lasting up to 1,000 ms, respectively. With a number of covariate factors incorporated into a prediction model, the eccentricity representation independently predicted the magnitude of post-activation suppression, which was more intense in regions representing more parafoveal visual fields compared to those of more peripheral fields. The initial negative component on VEP was sharply contoured and co-occurred with early high-gamma augmentation, whose offset then co-occurred with a large positive VEP peak. A delayed negative VEP peak was blunt and co-occurred with prolonged high-gamma attenuation.

*Corresponding Author: Eishi Asano, MD, PhD, MS (CRDSA), Professor of Pediatrics and Neurology & Medical Director of Neurodiagnostics, Department of Neurodiagnostics, Children's Hospital of Michigan, Wayne State University. 3901 Beaubien St., Detroit, MI, 48201, USA, Tel.: +1-313-745-5547, FAX: +1-313-745-9435, easano@med.wayne.edu.

CONFLICT OF INTEREST

None of the authors have potential conflicts of interest to be disclosed.

CONCLUSIONS—Eccentricity-dependent gradient in neural suppression in the medial-occipital region may explain the functional difference between peripheral and parafoveal/central vision. Early negative and positive VEP components may reflect neural activation, whereas a delayed negative VEP peak reflecting neural suppression.

SIGNIFICANCE—Our observation provides the mechanistic rationale for transient scotoma or mild flash-blindness, characterized by physiological afterimage formation preferentially in central vision following intense but non-injurious light exposure.

Keywords

high-frequency oscillations (HFOs); ripples; event-related high-gamma activity; pediatric epilepsy surgery; intracranial EEG recording; functional brain mapping; animation movie; photic stimulation; vision; perception; inhibition; deactivation

INTRODUCTION

Humans manage to live under the sun, and are repeatedly exposed to gross and extensive changes in low-level visual information in daily life. For example, you might remember that the sunlight dazzled your eyes when you stepped out from a movie theater. Experimental studies using visual-evoked potentials (VEP) and electrical stimulation suggest that such visual perception is associated primarily with neural processing in the medial-occipital region (Barett et al., 1976; Ducati et al., 1988; Winawer and Parvizi, 2016; Bosking et al., 2017). Electrophysiological studies of animals suggest that flash stimuli elicit neural activation in the striate cortex (also known as primary visual cortex or, simply, V1) within 100 ms after stimulus onset, as reflected by increased firing rate and augmentation of high-gamma activity above 70 Hz; in turn, the offset of visual stimuli elicits neural suppression as reflected by attenuation of high-gamma activity below the baseline level (Leopold and Logothetis, 1998; Ray and Maunsell, 2011). Studies of patients with focal epilepsy, using electrocorticography (ECoG), also replicated flash-related high-gamma augmentation followed by attenuation in the early visual cortex (Asano et al., 2009b; Matsuzaki et al., 2012). Yet, it still remains undetermined if there is a large-scale spatial difference across the human medial-occipital region in the dynamics of neural processing for full-field visual stimulation. We expect that functional difference, if present in an eccentricity-dependent manner, would improve our understanding of the early visual cortex for parafoveal and far peripheral fields. *How can we test this?* Quantitative measurement of neural responses from deep portions of the medial-occipital cortex may be difficult using noninvasive methods such as scalp EEG or magnetoencephalography. ECoG provides a unique opportunity of direct recording from the human cortical surface, but spatial sampling is generally limited in individual patients undergoing presurgical evaluation of focal epilepsy because extensive ECoG sampling from the nonepileptic striate cortex is frequently not feasible nor clinically warranted. Here, we overcame such limited spatial sampling, by combining ECoG signals derived from a large number of patients, each of whom had a small number of strip electrodes placed on the medial-occipital cortex which turned out to be non-epileptic following chronic ECoG monitoring. This approach allowed us to delineate visually-elicited neural modulations on a standard brain template in a four-dimensional manner. The main

goal of this study is to determine if the early visual cortex in the medial-occipital region would have eccentricity-dependent difference in visually-elicited high-gamma dynamics.

The second goal of this study is to determine the neural events underlying the components of VEP (American Clinical Neurophysiology Society, 2006; Odom et al., 2016). Both on scalp EEG and intracranial ECoG recording, normal VEP at the occipital lobe consists of a negative peak at a latency of <100 ms (referred to as N1 here), a positive peak around 100 ms (referred to as P2), and subsequently followed by a second, delayed negative peak (referred to as N3). VEP peak latencies are often utilized for clinical diagnosis, and it would be valuable to provide the empirical data addressing whether each VEP peak indeed reflects neural activation or suppression in human early visual cortex. As suggested in studies with monkeys (Wilke et al., 2006; Whittingstall and Logothetis, 2009), we hypothesized that the initial negative VEP component would co-occur with high-gamma augmentation, reflecting neural activation (Ray et al., 2008, Crone et al., 2011, Magri et al., 2012). Conversely, we hypothesize that the delayed VEP components would rather co-occur with high-gamma attenuation; thus, reflecting neural suppression.

MATERIALS AND METHODS

The inclusion criteria consisted of patients with focal epilepsy who underwent functional brain mapping using flash stimuli during extraoperative ECoG recording at Children's Hospital of Michigan or Harper University Hospital in Detroit. The exclusion criteria consisted of: (i) age younger than 4 years (Nakai et al., 2017), (ii) presence of massive cortical malformations affecting the calcarine, central or lateral sulcus, (iii) seizure onset zone, interictal spikes, or epileptogenic lesions involving the medial-occipital cortex (i.e.: lingual and cuneus gyri below and above the calcarine sulcus, respectively; Figure 1), and (iv) history of previous epilepsy surgery. Sixty-three patients satisfying the inclusion and exclusion criteria were studied (age range: 4–44 years; 32 females; Table 1). The study was approved by the Institutional Review Board at Wayne State University, and informed consent was obtained from the patients or guardians of patients.

Acquisition of ECoG and three-dimensional Magnetic Resonance (3D MR) surface images

The principal methods of ECoG and MRI data acquisition are identical to those previously reported (Nakai et al., 2017). Macro-electrodes (10 mm center-to-center distance; 4 mm diameter) were placed on the affected hemisphere for subsequent localization of the boundary between the epileptogenic zone and the eloquent cortex (Asano et al., 2009a). ECoG recordings were obtained, using Nihon Kohden Neurofax System (Nihon Kohden America Inc., Foothill Ranch, CA, USA) at a sampling frequency of 1,000 Hz. In order to maximize the generalizability of the findings, sites classified as seizure onset zone, epileptogenic lesions, as well as those showing interictal spikes or artifacts during the flash stimulation trials were excluded from further analysis (van 't Klooster et al., 2011; Zijlmans et al., 2012). Thus, a total of 6,337 electrodes were included in the further analyses. The following quantitative ECoG analyses were done with a band-pass filter of 0.08 to 300 Hz.

A 3D MR surface image was generated individually with the location of electrodes directly denoted on the cortical surface (Nakai et al., 2017). Individual electrode sites were spatially

normalized with FreeSurfer scripts (http://surfer.nmr.mgh.harvard.edu). All electrode sites were transformed into Talairach coordinates and plotted on the averaged FreeSurfer pial surface image, which has been validated in individuals of four years and above (Desikan et al., 2006; Ghosh et al., 2010; Nakai et al., 2017). Cortical gyri were parcellated at both individual and spatially normalized brain surfaces, and regions of interest (ROIs) are presented in Figure 1A. The medial-occipital cortex was defined to consist of the lingual and cuneus gyri, and the boundary of striate cortex was delineated according to the atlas which localized V1 using the stria of Gennari, as can be identified on MRI (Figure 1A; Hinds et al., 2008). The receptive-field eccentricity map in the medial-occipital cortex was determined using the retinotopy template based on the functional MRI (fMRI) study on 25 healthy subjects (Figure 1B; Benson et al., 2012; Griffis et al., 2015); the receptive field eccentricity map identifies the localization of a point in the visual field within the cortex as defined relative to the fovea, in degrees.

Direct cortical stimulation mapping

As part of presurgical evaluation, all patients underwent functional cortical mapping using electrical stimulation. The methods were previously described (Nakai et al., 2017). Electrical stimuli were delivered to neighboring electrode pairs, with frequency of 50 Hz, pulse duration of 300 μsec, and train duration ranging up to 5 s. Patients were aware of the timing but not the location of stimulation. As soon as patients exhibited a symptom, stimulation was terminated. The neuropsychologist, not being aware of the results of ECoG-based mapping, asked patients to describe the nature of visual perception, if any. Stimulus intensity was first set to 3 mA, and increased until a symptom or after-discharge was observed. The probability of stimulation-elicited phosphene (perception of a flash of light) and visual distortion (perception of visual changes other than light [e.g.: examiner's face appearing wavy or transparent]) was presented on the averaged FreeSurfer pial surface image (Figure 2).

Full-field flash stimuli

All patients were awake without sedation, comfortably seated in their hospital bed, and maintaining their eyes closed in a darkened room. Bio-monitoring systems were placed outside the patient's visual field and the eyes were closed throughout the session; thus, we assume that external visual stimuli other than flash transmission through the eyelid was effectively minimized, whereas complete darkness was not feasible. As part of our presurgical evaluation procedure, a series of 50 full-field flash stimuli were given with a frequency of 0.5 Hz, at a distance of 30 cm from the closed eyes, using the square-shape xenon photic stimulator LS-703A (Nihon Kohden America Inc). This stimulator has a field size of 13 × 3.5 cm, a maximum flash energy of 1.28 J, a flash duration of 20 μsec, and a mean luminance of 30,000 cd/m^2. The timing of each flash stimulus was integrated to the ECoG acquisition system via the TTL trigger signal generated at the onset of each flash.

Quantitative analysis of event-related high-gamma activity

Event-related high-gamma augmentation/attenuation is considered to be an excellent summary measure of neural activation/suppression, respectively (Tanji et al., 2005; Shmuel et al., 2006; Crone et al., 2011). We determined the temporal dynamics of high-gamma amplitude modulation for each electrode site as well as each region of interest (Figure 1).

Below, we defined high-gamma band as 70–110 Hz, based on the previous literature reporting that amplitude augmentation including this frequency band was concordant with sensorimotor-cognitive sites defined by electrical stimulation (for example, Wang et al., 2016; Nakai et al., 2017) and that removal of cortical sites showing such amplitude augmentation frequently resulted in clinically noteworthy deficits (Cervenka et al., 2013; Kojima et al., 2013a; 2013b).

The principal methods are identical to those previously reported (Nakai et al., 2017). No 60-Hz notch filter was used for analysis in any of the subjects. ECoG signals were transformed into the time-frequency domain in steps of 10 Hz and 5 ms, using a complex demodulation (Papp and Ktonas, 1977) incorporated in BESA software (BESA, Gräfelfing, Germany; Hoechstetter et al., 2004). The low-pass filter was a finite impulse response (FIR) filter of Gaussian shape; thus, making this complex demodulation effectively equivalent to a Gabor transform. The time-frequency resolution, defined as the 50% power drop of the finite impulse response filter, was ±7.9 ms and ±14.2 Hz, since the FIR filter had a full width at half maximum of 2 × 7.9 ms in the temporal domain and 2 × 14.2 Hz in the frequency domain. At each electrode site, we determined how much high-gamma amplitudes$_{70–110\ Hz}$ were increased or decreased, at each 5 ms epoch, compared to those during the reference period at 100–200 ms prior to stimulus onset. We delineated the percent change of high-gamma amplitudes, at each 5-ms epoch, at each electrode site with a Gaussian half-width at half maximum of 3 mm, and sequentially animated this on the average FreeSurfer pial surface image (Video S1 and Figure 3). We also presented the temporal change of high-gamma amplitudes in each ROI as a function of time (Figure 4).

Determination of the neuronal events underlying VEP peaks

We determined whether given VEP components in the early visual cortex were associated with neural activation reflected by non-phase-locked high-gamma augmentation or neural suppression reflected by high-gamma attenuation. VEP was measured at all electrode sites by averaging ECoG voltage traces time-locked to stimulus onset (American Clinical Neurophysiology Society, 2006; Odom et al., 2016); thus, high-gamma activity directly derived from VEP signal is time- and phase-locked across trials. Subsequently, we computed non-phase-locked high-gamma modulation by first removing VEP signal from the single trial time series (Tallon-Baudry et al., 1996; Fukuda et al., 2008; Figure 5).

At the medial- and lateral-occipital regions, we determined the temporal relationship between VEP components and non-phase-locked high-gamma modulations. VEP peaks of interest included: (i) N1 defined as the largest negative peak prior to P2, (ii) P2 defined as the largest positive peak occurring around 100 ms after stimulus onset, and (iii) N3 defined as the subsequent largest negative peak. Likewise, we determined the temporal relationship between VEP peaks and amplitude modulation of non-phase-locked low-frequency band activity$_{20–30\ Hz}$. Previous ECoG studies have suggested that event-related attenuation of ECoG activity at 8–32 Hz, as consistently reported to be elicited in the primary sensorimotor cortex during motor tasks, reflects mechanisms underlying facilitation of cortical processing (Crone et al., 1998; Miller et al., 2007).

Statistical analysis

With a linear mixed-model analysis incorporated in SPSS Statistics 24 (IBM Corp., Chicago, IL, USA), we determined whether flash-related high-gamma dynamics at each electrode site within the medial-occipital region differed according to the receptive-field eccentricity. The dependent variables included (1) the maximum augmentation of high-gamma amplitude as a measure reflecting the intensity of early neural excitation, and (2) the maximum attenuation of high-gamma amplitude reflecting the degree of post-activation suppression. The following 12 covariates were treated as fixed effects: (1) 'receptive-field eccentricity' (ranging from 2.2, 4.1, 7.3, 14.1, 25.5, to 40.0°; Figure 1), (2) 'patient age' (years), (3) 'gender' (1 if male and 0 otherwise), (4) 'sampled hemisphere' (1 if left), (5) 'lingual or cuneus' (1 if located within the lingual gyrus), (6) 'V1 location' (1 if located within the human V1 area based on Hinds et al., 2008), (7) 'stimulation-induced phosphene' (1 if positive), (8) 'stimulation-induced visual distortion' (1 if positive), (9) 'number of oral antiepileptic drugs' (reflecting the severity of seizure burden and related cognitive impairment; Kwan and Brodie, 2001), (10) 'primarily GABA-mediated antiepileptic medications' (1 if valproate, clobazam, or topiramate taken), (11) 'proximity to seizure onset zone' (1 if the seizure onset zone involved the lateral-occipital region), and (12) 'etiology' (1 if the underlying etiology was cortical dysplasia/brain malformation). We expected that incorporation of these covariates in the model would effectively determine if epileptic processes affected the neural processing in the medial-occipital cortex. 'Intercept for patient' was treated as a random effect. The level of significance was set at $p = 0.05$, and Bonferroni correction was employed for multiple comparisons (i.e.: two comparisons for two dependent variables).

In addition, a 3 × 3 Chi-square test determined if the probability of stimulation-elicited symptoms ('phosphene', 'visual distortion', or 'failure to elicit visual symptom') differed between the medial-occipital, lateral-occipital, and posterior-fusiform regions (Figure 2).

RESULTS

Results of electrical stimulation

Figure 2 presents 3D maps showing the probability of phosphene and visual distortion elicited by electrical stimulation at given sites. 146/265 (55.1%) electrodes in medial-occipital, 122/302 (40.4%) in lateral-occipital, and 10/188 (5.3%) in posterior-fusiform regions were classified as 'phosphene' sites, whereas 9/265 (3.4%) of medial-occipital, 11/302 (3.6%) of lateral-occipital, and 5/188 (2.7%) of posterior-fusiform regions were classified as 'visual distortion' sites. A 3 × 3 Chi-square test suggested that the probability of stimulation-elicited visual symptoms differed between three ROIs (Chi-square: 124.2; $p < 0.00001$). A phosphene was elicited preferentially by stimulation of medial- and lateral-occipital regions (Figure 2A), whereas the probability of visual distortion elicited by stimulation was comparable between three ROIs (Figure 2B).

Spatial-temporal dynamics of flash-related high-gamma modulation

Figure 3 and Video S1 present the dynamic changes of high-gamma activity elicited by full-field flash stimulation. Visual assessment indicates that high-gamma augmentation involved

the medial-occipital region by 80 ms after stimulus onset. High-gamma augmentation was modest in the lateral occipital and posterior-fusiform regions. High-gamma augmentation in the medial-occipital region was subsequently replaced by prolonged high-gamma attenuation lasting up to 1,000 ms following stimulus onset. Such delayed high-gamma attenuation was particularly prominent in the posterior portion of the striate cortex (Figures 3C and 3D).

Figure 4 summarizes the dynamics of flash-related high-gamma modulation in each ROI. The medial- and lateral-occipital regions showed rapid and brief high-gamma augmentation followed by prolonged high-gamma attenuation (Figures 4A and 4B), whereas high-gamma modulation in the posterior-fusiform region was modest (Figure 4C). An eccentricity-dependent gradient in the intensity of rapid high-gamma augmentation was not clearly delineated within the medial-occipital region (Figures 4D and 4E); indeed, the mixed model analysis failed to find an association between the receptive-field eccentricity and the degree of high-gamma augmentation [$t = 1.397$; $p = 0.164$]. The mixed model suggested that the maximum high-gamma amplitude was greater in medial-occipital sites within the human V1 area compared to those outside [Estimate = +0.511 (95%CI: +0.150 to +0.872); $t = 2.79$; $p = 0.006$], and that the maximum high-gamma amplitude was positively correlated to patient age [Estimate = +0.059 (95%CI: +0.014 to +0.104); $t = 2.679$; $p = 0.012$].

Conversely, the medial-occipital region showed a clear eccentricity-dependent gradient in the post-activation suppression rated by the maximum attenuation of high-gamma amplitude (Figures 4D and 4F). The mixed model analysis demonstrated that greater high-gamma attenuation was independently associated with smaller eccentricity [Estimate = −0.030 (95%CI: −0.042 to −0.019); $t = -5.113$; $p < 0.001$], localization within the human V1 area [Estimate = −0.060 (95%CI: −0.094 to −0.026); $t = -3.440$; $p = 0.001$], and areas where electrical stimulation induced phosphene [Estimate = −0.065 [95%CI: −0.110 to −0.020]; $t = -2.845$; $p = 0.005$]. To explore if the timing or intensity of early excitation would predict the intensity of post-activation suppression at given medial-occipital sites, an *ad-hoc* analysis was employed with the timing and intensity of maximum high-gamma augmentation included as co-variates. We found that neither timing ($t = -0.910$; $p = 0.364$) nor intensity ($t = 0.094$; $p = 0.925$) of maximum high-gamma augmentation predicted the upcoming maximum high-gamma attenuation.

Temporal relationship between VEP components and high-gamma/low-frequency band amplitude modulation

Figure 5 summarizes the temporal relationship between VEP peaks and modulations of non-phase-locked high-gamma/low-frequency band activity. Large proportions (64% and 65%) of early high-gamma augmentation was non-phase-locked in both medial- and lateral-occipital regions, respectively (Figure 5B). The N1 component roughly co-occurred with augmentation of non-phase-locked high-gamma activity, but the N1 peak latency preceded that of non-phase-locked high-gamma augmentation by 31 and 21 ms in medial- and lateral-occipital regions. The P2 peak co-occurred with the offset of non-phase-locked high-gamma augmentation, and the N3 peak co-occurred with high-gamma attenuation.

The vast majority of early augmentation of low-frequency band activity was phase-locked in both medial- and lateral-occipital regions, respectively (Figure 5C); in other words, the N1 component of the VEP consisted of much of the early low-frequency band augmentation. The P2 peak co-occurred with low-frequency band attenuation, whereas the N3 peak with delayed low-frequency band augmentation.

DISCUSSION

Full-field flash stimulation elicited brief neural activation reflected by high-gamma augmentation followed by prolonged suppression reflected by high-gamma attenuation in the early visual system. It provided evidence for a large-scale, eccentricity-dependent gradient in the intensity of post-activation suppression. Specifically, post-activation suppression was more intense in sites supporting more parafoveal representation relative to sites supporting a more peripheral representation (Figure 4E). Anatomically-defined V1 areas and those responsible for stimulation-induced phosphenes were also associated with post-activation suppression more intense compared to the surrounding areas. These effects were robust and independently significant even with a number of covariates incorporated into the prediction model.

Possible mechanism of high-gamma modulation

Our study is not designed to elucidate the cellular mechanism which fully explains the origin of flash-related high-gamma modulations. According to previously proposed models (Logothetis, 2003; Bartos et al., 2007; Ray et al., 2008; Trevelyan 2009; Ray and Maunsell, 2011; Whittington et al., 2011; Buzsáki and Wang, 2012; Lee and Jones, 2013; Scheffer-Teixeira et al., 2013; Suffczynski et al., 2014), the summation of action potentials and synaptic currents likely constitutes high-gamma augmentation. Here, about 35% of early high-gamma augmentation was contributed by the sharply-contoured N1 VEP component (Figure 5), reported to be associated with action potentials of pyramidal neurons (Ray and Maunsell, 2011). Non-phase-locked high-gamma augmentation, whose peak was preceded by N1 peak by 20–30 ms, might partly reflect interneuronal synaptic communications rapidly facilitated by excitation of pyramidal neurons (Markram et al., 2004; Kapfer et al., 2007).

Delayed and prolonged high-gamma attenuation perhaps reflects suppression of synaptic and action potential currents, largely triggered by GABAergic interneuronal communications. A study of monkeys showed that brief excitation of the lateral geniculate nucleus with a single-pulse micro-stimulation of 200μs duration resulted in a rapid increase in firing rate within striate cortex followed by suppression lasting for 300 ms (Logothetis et al., 2010). Simultaneous fMRI showed hemodynamic deactivation in the early visual system including V1, whereas injection of GABA antagonists prevented such hemodynamic deactivation; thus, they inferred that stimulation-induced deactivation results from synaptic inhibition. GABAergic interneuronal communications are believed to play a role in modulating the contrast and receptive field for optimal sensory perception (Sillito 1975; Dykes et al, 1984; Kapfer et al., 2007). A possibility not as of yet excluded is that post-activation suppression can be driven directly by activation of pyramidal cells; an optogenetic

study reported that activation of excitatory pyramidal neurons alone was sufficient to elicit post-activation suppression lasting up to 200 ms (Han et al., 2009). Our study demonstrated that post-activation suppression lasted for 1,000 ms particularly in the striate cortex supporting parafoveal vision; such prolonged suppression might be associated with our study design in which bright and full-field visual stimuli were employed.

Possible reasons for an eccentricity-dependent gradient in post-activation suppression

We do not have a definitive description of the underlying mechanism of eccentricity-dependent gradient in the intensity of high-gamma attenuation. It is plausible to hypothesize that uneven distribution of inhibitory neurons would be responsible for such spatial variance in post-activation suppression within the striate cortex. A previous study of the lateral geniculate nucleus and striate cortex of monkeys reported that the ratio of parvocellular to magnocellular projections increased by seven times from '5:1 in the 15° peripheral' to '35:1 in the foveal representation'. This parvocellular-to-magnocellular ratio was comparable to the ratio of Pβ to Pα ganglion cells in peripheral retina but far exceeded that of the central retina; this observation suggests that over-representation of parvocellular projections for central vision is enhanced at the cortical level (Azzopardi et al., 1999). Another study of the striate cortex of monkeys demonstrated that the 4Cβ layer receiving parvocellular projections had a 50% greater proportion of GABA-immunoreactive neurons compared to the 4Cα receiving magnocellular projections (Fitzpatrick et al., 1987).

Another hypothesis is that more peripheral V1 sites may receive feedforward signals from the lateral geniculate nucleus of the thalamus earlier than para-foveal sites, and may facilitate network inhibition more preferentially toward the central representation (Chagnac-Amitai and Connors, 1989; Schmolesky et al., 1998). If this hypothesis is correct, either timing or intensity of early activation would predict the intensity of post-activation suppression. Yet, our linear mixed model analysis suggested that neither high-gamma augmentation measure was predictive of the intensity of delayed high-gamma attenuation.

Since external visual stimuli other than full-field flash transmission through the eyelid was effectively minimized and no particular task was assigned, we estimate that the effect of the patient's attention on high-gamma measures was negligible in this study. If patients had attended involuntarily to the direction of the photic stimulator placed in front of them, such attention would have increased high-gamma amplitudes in the parafoveal representation of V1 (Fries et al., 2007; Jensen et al., 2007). Yet, our empirical ECoG measurement did not show parafoveal-preferential high-gamma augmentation (Figure 4E).

Significance of flash-related high-gamma modulation

Our observation of prolonged high-gamma attenuation in the striate cortex may provide the mechanistic rationale for transient scotoma or mild flash-blindness, characterized by physiological afterimage formation preferentially in the parafoveal/central vision for a few seconds following intense but non-injurious light exposure (Hamilton, 1968). For example, an airplane pilot may not be able to visualize a scene or instrument in front of him or her after being exposed to flashes of light for a brief moment. Transient loss of sensitivity of photoreceptors in the retina and constriction of the pupil have been considered to be the

primary cause of flash-blindness and loss of dark adaptation (Brown, 1965; Shimojo et al., 2001). The present study, in which external visual stimulus to the retina was limited to a flash of 20 μsec duration throughout the experiment, provided unique evidence that post-activation suppression at the cortical level could at least partly account for the physiological afterimage formation which occurs following exposure to full-field flashes of light.

It is recommend to divert central vision away from oncoming bright lights when driving to avoid transient blindness, and our data points to a central mechanism capable of explaining this phenomenon. Our observation of eccentricity-dependent post-activation suppression may reflect the different functional roles of central and peripheral vision. Central vision has greater acuity compared to peripheral vision; this is largely attributed to the cortical magnification that larger extents of the striate cortex are allocated to neural processing of central compared to peripheral vision (Schwartz, 1980; Hinds et al., 2008). Greater visual acuity in central vision may be also attributed to better contrast sensitivity in central vision, which has greater capability to disable neural activation laterally spreading toward neighboring sites; such lateral inhibition has been reported to be more intense for foveal compared to peripheral representation (Leat et al., 1999; Chung, 2004). An invasive study of patients with focal epilepsy suggested that the striate cortex can rapidly exert an inhibitory process, by reporting the stimulation results that the size of a perceived phosphene increases with stimulus intensity but rapidly reaches saturation (Bosking et al., 2017); we did not vary the intensity of our stimulus but anticipated that a flash luminance of 30,000 cd/m^2 should be sufficient to saturate this system, even when the eyes were closed. Less intense post-activation suppression in the peripheral representation is consistent with the notion that these striatal areas are more specialized to detect motion and speed (Yu et al., 2010). Shorter recovery of photosensitivity to the baseline level would be needed in optimal detection of objects within a constantly-changing environment as well as in control of rapid-aiming self-movements.

The present study demonstrated that flash-related high-gamma attenuation co-occurred with augmentation of low-frequency band activity$_{20–30\ Hz}$ in both striate and lateral occipital regions. One may hypothesize that such ECoG changes are, in part, associated with short-term visual memory maintenance function. A behavioral study reported that the strength of afterimage formation predicted subsequent short-term visual memory performance (Sligte et al., 2008). A previous ECoG study reported that a task requiring short-term visual memory function augmented extra-striatal beta activity$_{15–25\ Hz}$ during a 1,200-ms memory maintenance period (Tallon-Baudry et al., 2001). Further studies are warranted to determine what ECoG measures would best predict successful short-term visual memory.

Our observations indicate that measurement of flash-related high-gamma modulation on ECoG is useful to localize the primary visual cortex in epilepsy presurgical evaluation, whereas the diagnostic utility of intracranially-recorded flash-related VEP has been previously clarified by a study of intraoperative monitoring (Ota et al., 2010). We suggest that assessment of ECoG traces during flash stimulation may help investigators in differentiating physiological from pathological high-frequency oscillations (HFOs) in a posterior region. HFOs have been proposed as promising epilepsy biomarkers. It is generally assumed that HFOs generated in the seizure onset zone are more likely to be pathological

(Zijlmans et al., 2012), whereas those constantly elicited by sensorimotor/cognitive tasks are more likely to be physiological (Asano et al., 2013). As suggested in Figures 4 and 5, physiological high-gamma augmentation in the striatal cortex often stands out from the background activity and may be followed by prolonged attenuation. We recommend visual assessment of the temporal relationship between flash stimuli and ECoG waveforms, in case one finds intermittent augmentation of high-gamma activity in a region proximal to the primary visual cortex. This simple procedure is expected to decrease the risk of misinterpretation of physiological high-gamma augmentation as pathological HFOs.

Significance of VEP components

VEP consists of negative, then positive, followed by negative peaks, but its polarity *per se* does not clarify whether the neurotransmission reflected by each VEP component is excitatory or inhibitory (Luck, 2014). Our study inferred the direction of neuronal modulation associated with each VEP component, by correlating to the amplitude of non-phase-locked high-gamma activity. The amplitude of high-gamma activity is an excellent measure of neural activation, since it is tightly correlated to firing rate (Ray et al., 2008), hemodynamic activation on fMRI (Shmuel et al., 2006; Logothetis et al., 2010; Scheeringa et al., 2011; Saignavongs et al., 2017), and glucose metabolism on positron emission tomography (Nishida et al., 2008). Conversely, the amplitude of alpha-beta activity at 10–30 Hz was reported to negatively correlate with hemodynamic responses (Scheeringa et al., 2011). The present study found that the N1 component roughly co-occurred with augmentation of non-phase-locked high-gamma activity, suggesting that this VEP component reflects neural activation. A previous study of monkeys indeed reported association between the N1 component and action potentials (Ray and Maunsell, 2011). Our observations of P2 peak co-occurring with low-frequency band attenuation and the offset of non-phase-locked high-gamma augmentation suggest that VEP waveforms before P2 peak latency may reflect neural activation. Most interestingly, the N3 component was associated with attenuation of high-gamma activity as well as augmentation of non-phase-locked low-frequency band activity; thus, negative VEP waveforms at 300 ms and after the stimulus onset are inferred to reflect neural deactivation. We believe that the aforementioned findings are useful for investigators to interpret long-latency event-related potentials generated by the striate cortex.

Supplementary Material

Refer to Web version on PubMed Central for supplementary material.

Acknowledgments

This work was supported by NIH grant NS064033 and R01 NS089659. We are grateful to Sandeep Sood, MD, Robert Rothermel, PhD, and Alanna Carlson, MS, LLP, at Children's Hospital of Michigan, Detroit Medical Center, Wayne State University for the collaboration and assistance in performing the studies described above.

References

American Clinical Neurophysiology Society. Guideline 9B: Guidelines on visual evoked potentials. J Clin Neurophysiol. 2006; 23:138–56. [PubMed: 16612231]

Asano E, Juhász C, Shah A, Sood S, Chugani HT. Role of subdural electrocorticography in prediction of long-term seizure outcome in epilepsy surgery. Brain. 2009a; 132:1038–47. [PubMed: 19286694]

Asano E, Nishida M, Fukuda M, Rothermel R, Juhász C, Sood S. Differential visually-induced gamma-oscillations in human cerebral cortex. Neuroimage. 2009b; 45:477–89. [PubMed: 19135157]

Asano E, Brown EC, Juhász C. How to establish causality in epilepsy surgery. Brain Dev. 2013; 35:706–20. [PubMed: 23684007]

Azzopardi P, Jones KE, Cowey A. Uneven mapping of magnocellular and parvocellular projections from the lateral geniculate nucleus to the striate cortex in the macaque monkey. Vision Res. 1999; 39:2179–89. [PubMed: 10343800]

Barett G, Blumhardt L, Halliday AM, Halliday E, Kriss A. A paradox in the lateralisation of the visual evoked response. Nature. 1976; 261:253–5. [PubMed: 1272400]

Bartos M, Vida I, Jonas P. Synaptic mechanisms of synchronized gamma oscillations in inhibitory interneuron networks. Nat Rev Neurosci. 2007; 8:45–56. [PubMed: 17180162]

Benson NC, Butt OH, Datta R, Radoeva PD, Brainard DH, Aguirre GK. The retinotopic organization of striate cortex is well predicted by surface topology. Curr Biol. 2012; 22:2081–5. [PubMed: 23041195]

Bosking WH, Sun P, Özker M, Pei X, Foster BL, Beauchamp MS, et al. Saturation in phosphene size with increasing current levels delivered to human visual cortex. J Neurosci. 2017; 37:7188–97. [PubMed: 28652411]

Brown JL. Flash blindness. Am J Ophthalmol. 1965; 60:505–20. [PubMed: 5825155]

Buzsáki G, Wang XJ. Mechanisms of gamma oscillations. Annu Rev Neurosci. 2012; 35:203–25. [PubMed: 22443509]

Cervenka MC, Corines J, Boatman-Reich DF, Eloyan A, Sheng X, Franaszczuk PJ, et al. Electrocorticographic functional mapping identifies human cortex critical for auditory and visual naming. Neuroimage. 2013; 69:267–76. [PubMed: 23274183]

Chagnac-Amitai Y, Connors BW. Horizontal spread of synchronized activity in neocortex and its control by GABA-mediated inhibition. J Neurophysiol. 1989; 61:747–58. [PubMed: 2542471]

Chung ST. Reading speed benefits from increased vertical word spacing in normal peripheral vision. Optom Vis Sci. 2004; 81:525–35. [PubMed: 15252352]

Crone NE, Miglioretti DL, Gordon B, Sieracki JM, Wilson MT, Uematsu S, et al. Functional mapping of human sensorimotor cortex with electrocorticographic spectral analysis. I. Alpha and beta event-related desynchronization. Brain. 1998; 121:2271–99. [PubMed: 9874480]

Crone NE, Korzeniewska A, Franaszczuk PJ. Cortical γ responses: searching high and low. Int J Psychophysiol. 2011; 79:9–15. [PubMed: 21081143]

Desikan RS, Ségonne F, Fischl B, Quinn BT, Dickerson BC, Blacker D, et al. An automated labeling system for subdividing the human cerebral cortex on MRI scans into gyral based regions of interest. Neuroimage. 2006; 31:968–80. [PubMed: 16530430]

Ducati A, Fava E, Motti ED. Neuronal generators of the visual evoked potentials: intracerebral recording in awake humans. Electroencephalogr Clin Neurophysiol. 1988; 71:89–99. [PubMed: 2449338]

Dykes RW, Landry P, Metherate R, Hicks TP. Functional role of GABA in cat primary somatosensory cortex: shaping receptive fields of cortical neurons. J Neurophysiol. 1984; 52:1066–93. [PubMed: 6151590]

Fitzpatrick D, Lund JS, Schmechel DE, Towles AC. Distribution of GABAergic neurons and axon terminals in the macaque striate cortex. J Comp Neurol. 1987; 264:73–91. [PubMed: 3680625]

Fries P, Nikoli D, Singer W. The gamma cycle. Trends Neurosci. 2007; 30:309–16. [PubMed: 17555828]

Fukuda M, Nishida M, Juhász C, Muzik O, Sood S, Chugani HT, et al. Short-latency median-nerve somatosensory-evoked potentials and induced gamma-oscillations in humans. Brain. 2008; 131:1793–805. [PubMed: 18508784]

Ghosh SS, Kakunoori S, Augustinack J, Nieto-Castanon A, Kovelman I, Gaab N, et al. Evaluating the validity of volume-based and surface-based brain image registration for developmental cognitive

neuroscience studies in children 4 to 11 years of age. Neuroimage. 2010; 53:85–93. [PubMed: 20621657]

Griffis JC, Elkhetali AS, Burge WK, Chen RH, Visscher KM. Retinotopic patterns of background connectivity between V1 and fronto-parietal cortex are modulated by task demands. Front Hum Neurosci. 2015; 9:338. [PubMed: 26106320]

Hamilton JE. The flashblindness problem in the aircraft cockpit. Am J Optom Arch Am Acad Optom. 1968; 45:86–95. [PubMed: 5236217]

Han X, Qian X, Bernstein JG, Zhou HH, Franzesi GT, Stern P, et al. Millisecond-timescale optical control of neural dynamics in the nonhuman primate brain. Neuron. 2009; 62:191–98. [PubMed: 19409264]

Hinds OP, Rajendran N, Polimeni JR, Augustinack JC, Wiggins G, Wald LL, et al. Accurate prediction of V1 location from cortical folds in a surface coordinate system. Neuroimage. 2008; 39:1585–99. [PubMed: 18055222]

Hoechstetter K, Bornfleth H, Weckesser D, Ille N, Berg P, Scherg M. BESA source coherence: a new method to study cortical oscillatory coupling. Brain Topogr. 2004; 16:233–8. [PubMed: 15379219]

Jensen O, Kaiser J, Lachaux JP. Human gamma-frequency oscillations associated with attention and memory. Trends Neurosci. 2007; 30:317–24. [PubMed: 17499860]

Kapfer C, Glickfeld LL, Atallah BV, Scanziani M. Supralinear increase of recurrent inhibition during sparse activity in the somatosensory cortex. Nat Neurosci. 2007; 10:743–53. [PubMed: 17515899]

Kojima K, Brown EC, Matsuzaki N, Rothermel R, Fuerst D, Shah A, et al. Gamma activity modulated by picture and auditory naming tasks: intracranial recording in patients with focal epilepsy. Clin Neurophysiol. 2013a; 124:1737–44. [PubMed: 23688918]

Kojima K, Brown EC, Rothermel R, Carlson A, Fuerst D, Matsuzaki N, et al. Clinical significance and developmental changes of auditory-language-related gamma activity. Clin Neurophysiol. 2013b; 124:857–69. [PubMed: 23141882]

Kwan P, Brodie MJ. Neuropsychological effects of epilepsy and antiepileptic drugs. Lancet. 2001; 357:216–22. [PubMed: 11213111]

Leat SJ, Li W, Epp K. Crowding in central and eccentric vision: the effects of contour interaction and attention. Invest Ophthalmol Vis Sci. 1999; 40:504–12. [PubMed: 9950611]

Lee S, Jones SR. Distinguishing mechanisms of gamma frequency oscillations in human current source signals using a computational model of a laminar neocortical network. Front Hum Neurosci. 2013; 7:869. [PubMed: 24385958]

Leopold DA, Logothetis NK. Microsaccades differentially modulate neural activity in the striate and extrastriate visual cortex. Exp Brain Res. 1998; 123:341–5. [PubMed: 9860273]

Logothetis NK. The underpinnings of the BOLD functional magnetic resonance imaging signal. J Neurosci. 2003; 23:3963–71. [PubMed: 12764080]

Logothetis NK, Augath M, Murayama Y, Rauch A, Sultan F, Goense J, et al. The effects of electrical microstimulation on cortical signal propagation. Nat Neurosci. 2010; 13:1283–91. [PubMed: 20818384]

Luck, SJ. An introduction to the event-related potential technique. 2. Cambrigde, MA: MIT press; 2014.

Magri C, Schridde U, Murayama Y, Panzeri S, Logothetis NK. The amplitude and timing of the BOLD signal reflects the relationship between local field potential power at different frequencies. J Neurosci. 2012; 32:1395–1407. [PubMed: 22279224]

Markram H, Toledo-Rodriguez M, Wang Y, Gupta A, Silberberg G, Wu C. Interneurons of the neocortical inhibitory system. Nat Rev Neurosci. 2004; 5:793–807. [PubMed: 15378039]

Matsuzaki N, Nagasawa T, Juhász C, Sood S, Asano E. Independent predictors of neuronal adaptation in human primary visual cortex measured with high-gamma activity. Neuroimage. 2012; 59:1639–46. [PubMed: 21945696]

Miller KJ, Leuthardt EC, Schalk G, Rao RP, Anderson NR, Moran DW, et al. Spectral changes in cortical surface potentials during motor movement. J Neurosci. 2007; 27:2424–32. [PubMed: 17329441]

Nakai Y, Jeong JW, Brown EC, Rothermel R, Kojima K, Kambara T, et al. Three- and four-dimensional mapping of speech and language in patients with focal epilepsy. Brain. 2017; 140:1351–70. [PubMed: 28334963]

Nishida M, Juhász C, Sood S, Chugani HT, Asano E. Cortical glucose metabolism positively correlates with gamma-oscillations in nonlesional focal epilepsy. Neuroimage. 2008; 42:1275–84. [PubMed: 18652902]

Odom JV, Bach M, Brigell M, Holder GE, McCulloch DL, Mizota A, et al. International Society for Clinical Electrophysiology of Vision. ISCEV standard for clinical visual evoked potentials: (2016 update). Doc Ophthalmol. 2016; 133:1–9.

Ota T, Kawai K, Kamada K, Kin T, Saito N. Intraoperative monitoring of cortically recorded visual response for posterior visual pathway. J Neurosurg. 2010; 112:285–94. [PubMed: 19630493]

Papp N, Ktonas P. Critical evaluation of complex demodulation techniques for the quantification of bioelectrical activity. Biomed Sci Instrum. 1977; 13:135–45. [PubMed: 871500]

Ray S, Crone NE, Niebur E, Franaszczuk PJ, Hsiao SS. Neural correlates of high-gamma oscillations (60–200 Hz) in macaque local field potentials and their potential implications in electrocorticography. J Neurosci. 2008; 28:11526–36. [PubMed: 18987189]

Ray S, Maunsell JH. Different origins of gamma rhythm and high-gamma activity in macaque visual cortex. PLoS Biol. 2011; 9(4):e1000610.doi: 10.1371/journal.pbio.1000610 [PubMed: 21532743]

Saignavongs M, Ciumas C, Petton M, Bouet R, Boulogne S, Rheims S, et al. Neural Activity Elicited by a Cognitive Task can be Detected in Single-Trials with Simultaneous Intracerebral EEG-fMRI Recordings. Int J Neural Syst. 2017; 27:1750001. [PubMed: 27718767]

Scheeringa R, Fries P, Petersson KM, Oostenveld R, Grothe I, Norris DG, et al. Neuronal dynamics underlying high- and low-frequency EEG oscillations contribute independently to the human BOLD signal. Neuron. 2011; 69:572–83. [PubMed: 21315266]

Scheffer-Teixeira R, Belchior H, Leão RN, Ribeiro S, Tort AB. On high-frequency field oscillations (>100 Hz) and the spectral leakage of spiking activity. J Neurosci. 2013; 33:1535–9. [PubMed: 23345227]

Schmolesky MT, Wang Y, Hanes DP, Thompson KG, Leutgeb S, Schall JD, et al. Signal timing across the macaque visual system. J Neurophysiol. 1998; 79:3272–8. [PubMed: 9636126]

Schwartz EL. Computational anatomy and functional architecture of striate cortex: a spatial mapping approach to perceptual coding. Vision Res. 1980; 20:645–69. [PubMed: 7445436]

Shimojo S, Kamitani Y, Nishida S. Afterimage of perceptually filled-in surface. Science. 2001; 293:1677–80. [PubMed: 11533495]

Shmuel A, Augath M, Oeltermann A, Logothetis NK. Negative functional MRI response correlates with decreases in neuronal activity in monkey visual area V1. Nat Neurosci. 2006; 9:569–77. [PubMed: 16547508]

Sillito AM. The contribution of inhibitory mechanisms to the receptive field properties of neurones in the striate cortex of the cat. J Physiol. 1975; 250:305–29. [PubMed: 1177144]

Sligte IG, Scholte HS, Lamme VA. Are there multiple visual short-term memory stores? PLoS One. 2008; 3:e1699. [PubMed: 18301775]

Suffczynski P, Crone NE, Franaszczuk PJ. Afferent inputs to cortical fast-spiking interneurons organize pyramidal cell network oscillations at high-gamma frequencies (60–200 Hz). J Neurophysiol. 2014; 112:3001–11. [PubMed: 25210164]

Tallon-Baudry C, Bertrand O, Delpuech C, Pernier J. Stimulus specificity of phase-locked and non-phase-locked 40 Hz visual responses in human. J Neurosci. 1996; 16:4240–9. [PubMed: 8753885]

Tallon-Baudry C, Bertrand O, Fischer C. Oscillatory synchrony between human extrastriate areas during visual short-term memory maintenance. J Neurosci. 2001; 21:RC177. [PubMed: 11588207]

Tanji K, Suzuki K, Delorme A, Shamoto H, Nakasato N. High-frequency gamma-band activity in the basal temporal cortex during picture-naming and lexical-decision tasks. J Neurosci. 2005; 25:3287–93. [PubMed: 15800183]

Trevelyan AJ. The direct relationship between inhibitory currents and local field potentials. J Neurosci. 2009; 29:15299–307. [PubMed: 19955382]

van ‘t Klooster MA, Zijlmans M, Leijten FS, Ferrier CH, van Putten MJ, Huiskamp GJ. Time-frequency analysis of single pulse electrical stimulation to assist delineation of epileptogenic cortex. Brain. 2011; 134:2855–66. [PubMed: 21900209]

Wang Y, Fifer MS, Flinker A, Korzeniewska A, Cervenka MC, Anderson WS, et al. Spatial-temporal functional mapping of language at the bedside with electrocorticography. Neurology. 2016; 86:1181–9. [PubMed: 26935890]

Whittingstall K, Logothetis NK. Frequency-band coupling in surface EEG reflects spiking activity in monkey visual cortex. Neuron. 2009; 64:281–9. [PubMed: 19874794]

Whittington MA, Cunningham MO, LeBeau FE, Racca C, Traub RD. Multiple origins of the cortical γ rhythm. Dev Neurobiol. 2011; 71:92–106. [PubMed: 21154913]

Wilke M, Logothetis NK, Leopold DA. Local field potential reflects perceptual suppression in monkey visual cortex. Proc Natl Acad Sci U S A. 2006; 103:17507–12. [PubMed: 17088545]

Winawer J, Parvizi J. Linking Electrical Stimulation of Human Primary Visual Cortex, Size of Affected Cortical Area, Neuronal Responses, and Subjective Experience. Neuron. 2016; 92:1213–9. [PubMed: 27939584]

Yu HH, Verma R, Yang Y, Tibballs HA, Lui LL, Reser DH, et al. Spatial and temporal frequency tuning in striate cortex: functional uniformity and specializations related to receptive field eccentricity. Eur J Neurosci. 2010; 31:1043–62. [PubMed: 20377618]

Zijlmans M, Jiruska P, Zelmann R, Leijten FS, Jefferys JG, Gotman J. High-frequency oscillations as a new biomarker in epilepsy. Ann Neurol. 2012; 71:169–78. [PubMed: 22367988]

HIGHLIGHTS

1. We generated a 4D map of neuronal modulations elicited by full-field photic stimulation.
2. The visual cortex showed an eccentricity-dependent gradient in the post-activation suppression.
3. Our unique ECoG dataset effectively clarified the neuronal events underlying VEP components.

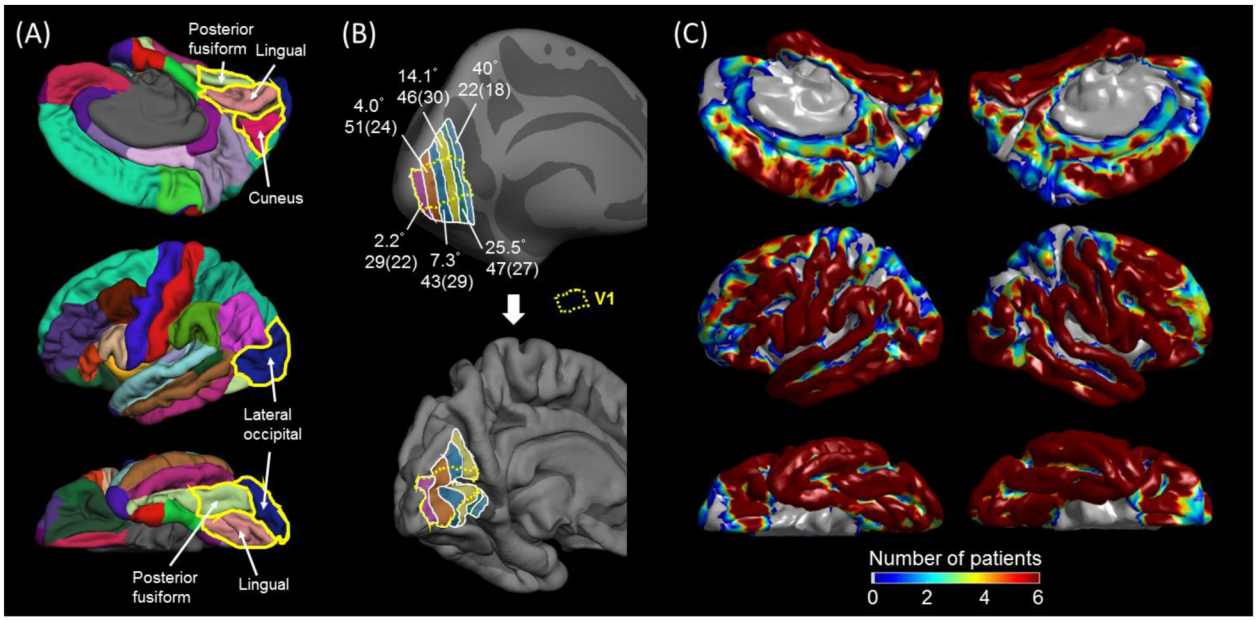

Figure 1. Regions of interest (ROIs), eccentricity estimates, and distribution of subdural electrodes

(A) The medial-occipital cortex was defined to consist of the lingual (pink; below the calcarine sulcus) and cuneus regions (wine red; above the calcarine sulcus). The lateral occipital (blue) and posterior fusiform regions (light green) were defined as previously reported (Desikan et al., 2006; Nakai et al., 2017). (B) The inflated (upper) and pial (lower) images of the left hemisphere of the FreeSurfer averaged brain denote the medial-occipital regions with mean receptive-field eccentricity of 2.2, 4.1, 7.3, 14.1, 25.5, and 40.0° (Benson et al., 2012; Griffis et al., 2015). The boundary of striate cortex (V1; Hinds et al., 2008) in the medial-occipital surface is delineated with a broken line. The number of analyzed electrodes within a given eccentricity region for either hemisphere is indicated (along with number of contributing patients in parentheses). (C) The distribution of subdural electrodes, included in further analyses, is indicated at the whole-brain level. It should be noted that subdural disk electrodes inherently fail to sample ECoG activities generated by the deep cortex along the calcarine sulcus.

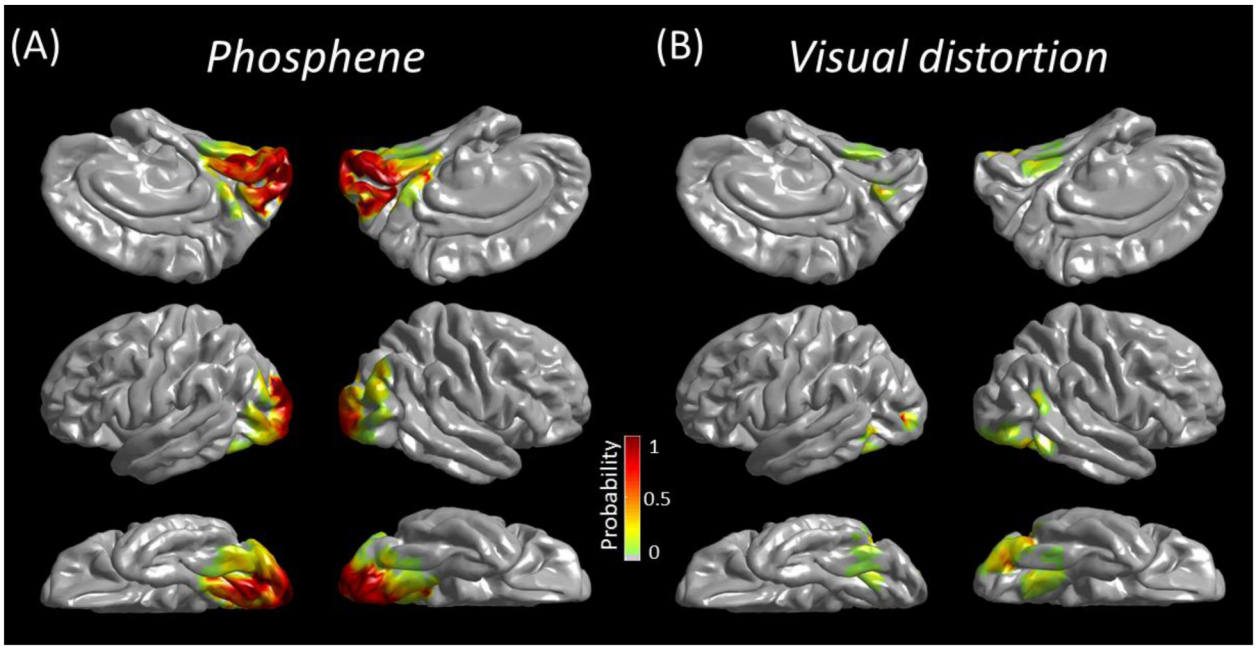

Figure 2. 3D probabilistic maps of visual function based on the results of electrical stimulation
(A) Phosphene. (B) Visual distortion.

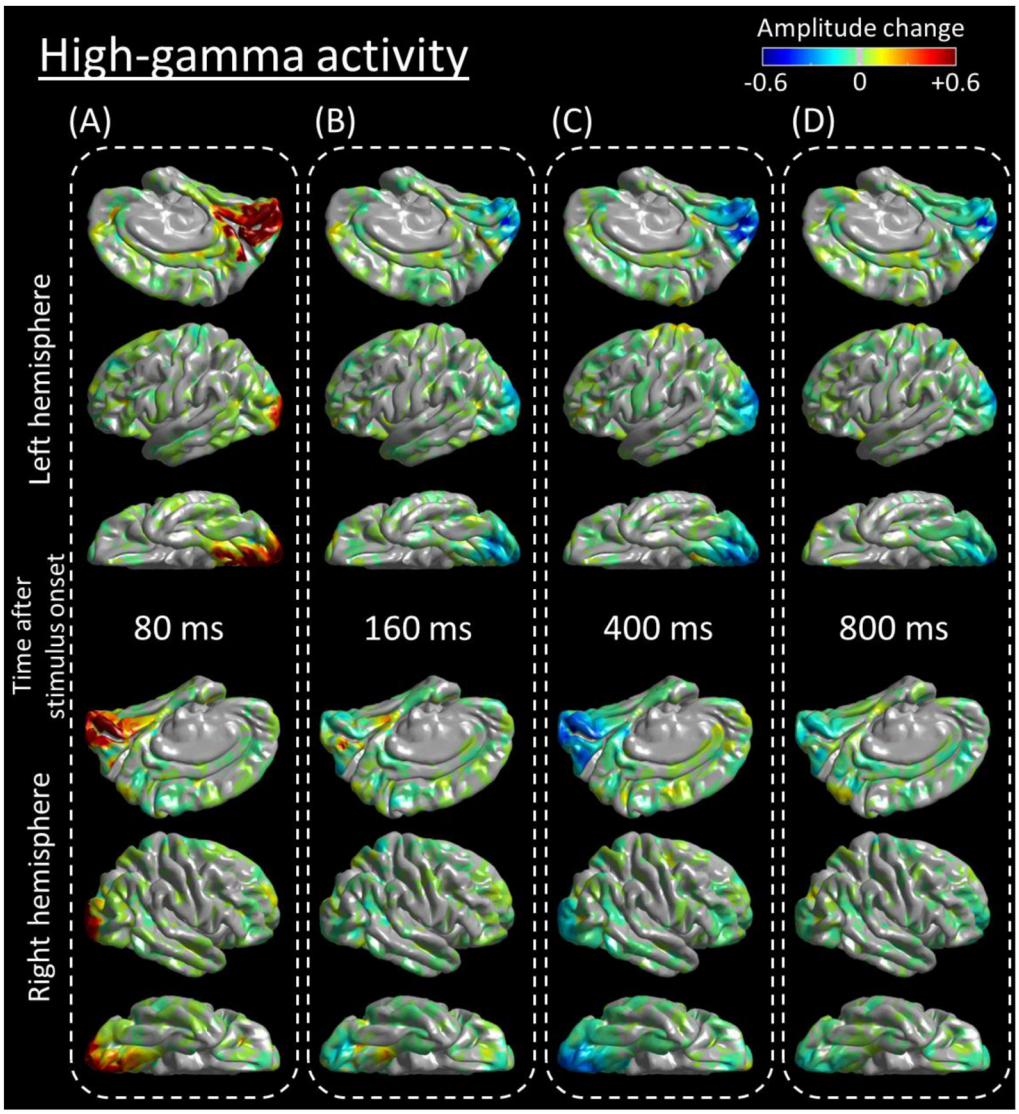

Figure 3. Snap shots of a 4D map of the human early visual system

Flash-related amplitude augmentation is reflected by red, whereas attenuation by blue color (See also Video S1). '+0.6' indicates that high-gamma amplitude$_{70–110Hz}$ was augmented by 60% compared to the average during the reference period at −200 to −100 ms relative to stimulus onset. Snapshots at (A) 80 ms, (B) 160 ms, (C) 400 ms, and (D) 800 ms.

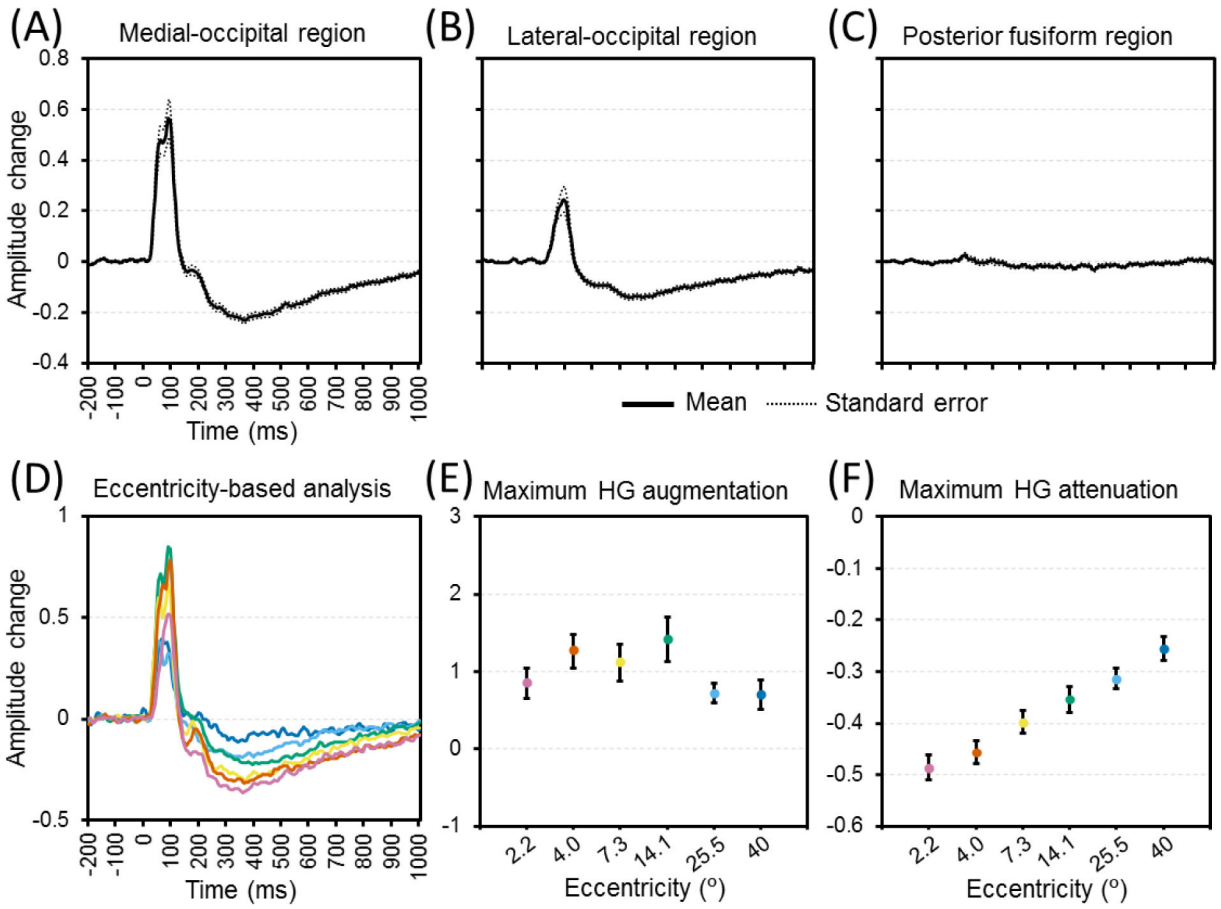

Figure 4. The temporal dynamics of flash-related high-gamma activity in each region of interest (ROI)

(A) Medial-occipital region. (B) Lateral-occipital region. (C) Posterior-fusiform region. High-gamma amplitudes are averaged for each region (including both hemispheres) and presented with standard errors. '+0.2' indicates that high-gamma amplitude was augmented by 20% compared to the average during the reference period. (D) The temporal dynamics of medial-occipital high-gamma amplitude at eccentricity-defined ROIs are presented (purple: 2.2; brown: 4.0; yellow: 7.3; green: 14.1; light blue: 25.5; blue: 40°). (E) The maximum augmentation of medial-occipital high-gamma (HG) amplitude. (F) The maximum attenuation of high-gamma amplitude following medial-occipital high-gamma augmentation.

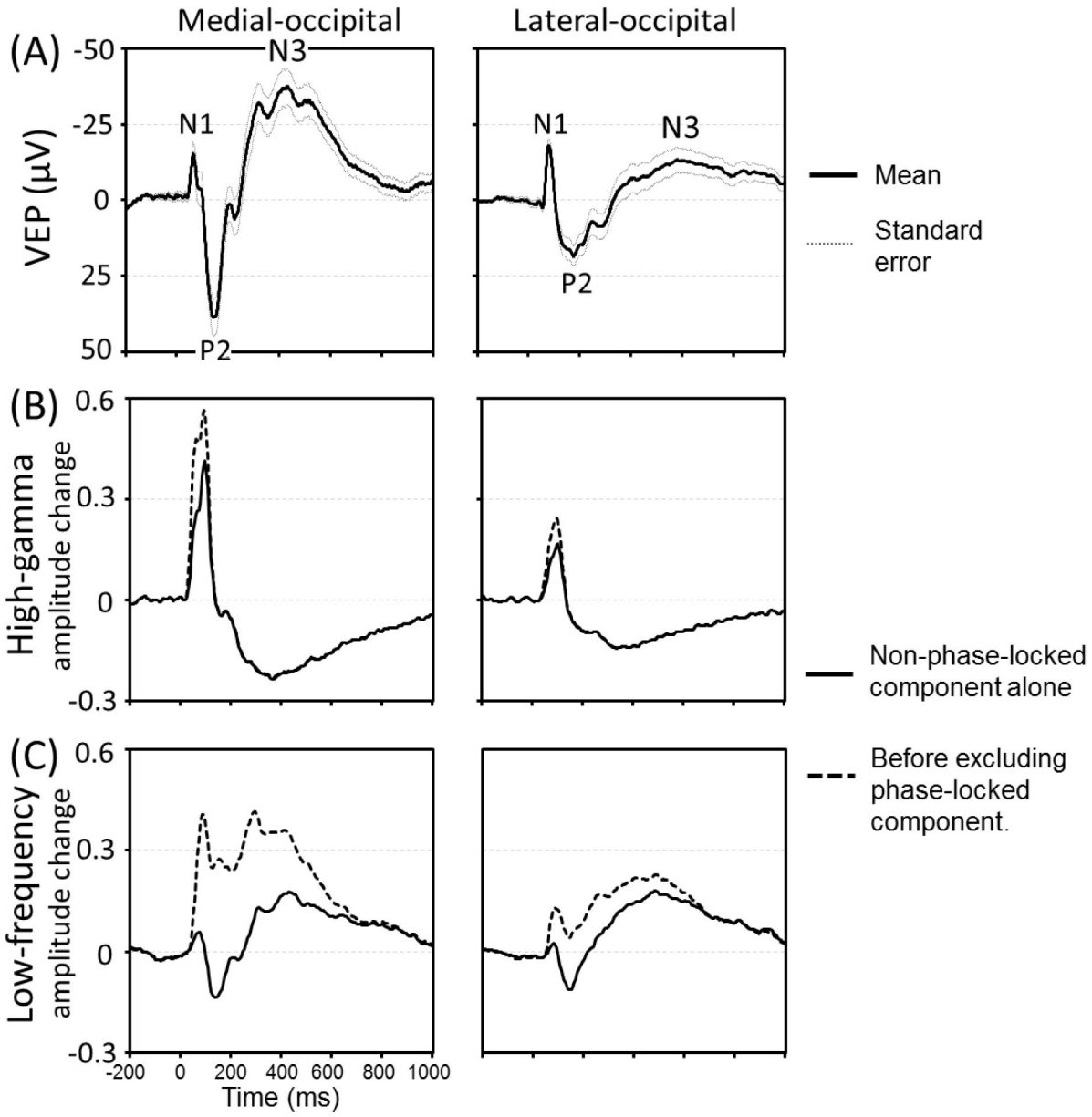

Figure 5. Visual-evoked potentials (VEPs), flash-related modulation of high-gamma and low-frequency band activity

(A) Grand-averaged VEPs at the medial- and lateral-occipital regions are presented with standard errors. N1 peak latency was 64 and 79 ms, P2 latency was 142 and 176 ms, and N3 latency was 430 and 580 ms in the medial- and lateral-occipital regions, respectively. (B) The temporal changes of high-gamma amplitudes are presented. Solid line: non-phase-locked components alone. Dotted line: High-gamma amplitudes before excluding phase-locked components. The peak latency of non-phase-locked high-gamma augmentation was 95 and 100 ms, respectively. (C) The temporal changes of low-frequency band amplitudes.

TABLE 1

Patient profile.

Number of patients	63
Mean age (year old)	13.5
Range of age (year old)	4 – 44
Proportion of male (%)	49.2
Sampled hemisphere. Number of patients (%)	
Left alone	25 (39.7)
Right alone	28 (44.4)
Both	10 (15.9)
Seizure onset zone. Number of patients (%)	
involving Frontal	12 (19.0)
involving Temporal	33 (52.4)
involving Parietal	16 (25.4)
involving Lateral-Occipital	4 (6.3)
Mean number of antiepileptic drugs	1.9
Antiepileptic drugs. Number of patients (%)	
Carbamazepine (CBZ)	4 (6.3)
Oxcarbazepine (OXC)	30 (47.6)
Lacosamide (LCM)	20 (31.7)
Zonisamide (ZNS)	4 (6.3)
Phenytoin (PHT)	2 (3.2)
Lamotrigine (LTG)	18 (28.6)
Levetiracetam (LEV)	24 (38.1)
Valproate (VPA)	8 (12.7)
Clobazam (CLB)	5 (7.9)
Topiramate (TPM)	2 (3.2)
Etiology. Number of patients (%)	
Tumor	12 (19.0)
Dysplasia	21 (33.3)
Hippocampal sclerosis	6 (9.5)
Dysplasia + Hippocampal sclerosis	1 (1.6)
No definitive lesion other than gliosis	22 (34.9)
Arteriovenous malformation	1 (1.6)

Ten patients had seizure onset zones involving at least two lobes.